Site-Specific Antibody Fragment Conjugates for Reversible Staining in Fluorescence Microscopy

Jonathan Schwach,[a] Ksenia Kolobynina,[b] Katharina Brandstetter,[a] Marcus Gerlach,[c] Philipp Ochtrop,[d] Jonas Helma,[c] Christian P. R. Hackenberger,[d, e] Hartmann Harz,[a] M. Cristina Cardoso,[b] Heinrich Leonhardt,[a] and Andreas Stengl*[a]

Antibody conjugates have taken a great leap forward as tools in basic and applied molecular life sciences that was enabled by the development of chemoselective reactions for the site-specific modification of proteins. Antibody-oligonucleotide conjugates combine the antibody's target specificity with the reversible, sequence-encoded binding properties of oligonucleotides like DNAs or peptide nucleic acids (PNAs), allowing sequential imaging of large numbers of targets in a single specimen. In this report, we use the Tub-tag® technology in combination with Cu-catalyzed azide-alkyne cycloaddition for the site-specific conjugation of single DNA and PNA strands to an eGFP-binding nanobody. We show binding of the conjugate to recombinant eGFP and subsequent sequence-specific annealing of fluorescently labelled imager strands. Furthermore, we reversibly stain eGFP-tagged proteins in human cells, thus demonstrating the suitability of our conjugation strategy to generate antibody-oligonucleotides for reversible immunofluorescence imaging.

Introduction

Proteins, especially antibodies, have been widely used as important tools in basic research and more recently as diagnostic and therapeutic agents.[1,2] Site- or residue-specific modification of antibodies with additional moieties ranging from small chemical compounds to large polypeptides has further expanded their field of use. This advancement was enabled by the development of chemoselective or bioorthogonal reactions and incorporation of unnatural amino acids into antibodies.[3] Antibody-oligonucleotide conjugates represent particularly interesting modalities, as they combine two key advantages of their building blocks in a single entity: specific antigen binding of antibodies with sequence-dependent hybridization of oligonucleotides to complementary strands. The former allows specific binding of target proteins in complex contexts such as cells, while the latter can be used for tunable, thus, reversible attachment of additional functionalities such as fluorophores. Unsurprisingly, protein-oligonucleotide conjugates have seen great use in a variety of applications ranging from protein immobilization,[4] bioanalytics[5–7] to material science.[8–10] Moreover, antibody-oligonucleotide conjugates have been employed in fluorescence and super resolution microscopy[11,12] as they resolve the limitations that come with standard fluorophore-conjugated antibodies.

Although fluorophore-conjugated antibodies are one of the most common staining reagents due to their broad spectrum of targets, the virtually irreversible binding of antibodies and the spectral overlap between fluorophores heavily limit the number of individual targets that can be investigated at the same time. To overcome this problem, efforts have been devoted to develop protocols to either elute the antibodies[13,14] or chemically inactivate the fluorophores in between successive imaging rounds. However, these techniques involve harsh washing steps and thereby potentially alter epitope accessibility for the following imaging probes. Thus, elution of the previous probe should ideally be rapid and buffer conditions mild to preserve sample integrity. An elegant way to achieve this goal was developed for super-resolution microscopy called DNA-point accumulation for imaging in nanoscale topography (DNA-PAINT).[15] DNA-PAINT exploits the transient binding of fluorophore-coupled oligonucleotides (imager strands) to their complementary sequence (docking strands) for reversible immobilization. The tunability of the binding strength between

[a] J. Schwach, K. Brandstetter, Dr. H. Harz, Prof. Dr. H. Leonhardt, Dr. A. Stengl
Ludwig-Maximilians-Universität München
Department of Biology II, Human Biology and BioImaging
82152 Planegg-Martinsried (Germany)
E-mail: stengl@bio.lmu.de
stengl.andreas@gmail.com
[b] K. Kolobynina, Prof. Dr. M. C. Cardoso
Technical University of Darmstadt
Department of Biology, Cell Biology and Epigenetics
Schnittspahnstr. 10, 64287 Darmstadt (Germany)
[c] Dr. M. Gerlach, Dr. J. Helma
Tubulis GmbH, BioSysM
Butenandtstrasse 1, 81377 Munich (Germany)
[d] P. Ochtrop, Prof. Dr. C. P. R. Hackenberger
Leibniz-Forschungsinstitut für Molekulare Pharmakologie (FMP)
Department Chemical Biology
Robert-Rössle-Strasse 10, 13125 Berlin (Germany)
[e] Prof. Dr. C. P. R. Hackenberger
Humboldt Universität zu Berlin
Department of Chemistry
Brook-Taylor-Strasse 2, 12489 Berlin (Germany)

Supporting information for this article is available on the WWW under https://doi.org/10.1002/cbic.202000727

This article is part of a joint Special Collection with the Journal of Peptide Science on SPP 1623: Chemoselective reactions for the synthesis and application of functional proteins. Please see our homepage for more articles in the collection.

oligonucleotides allows for rapid exchange of fluorophores under mild washing conditions.[16,17]

Techniques to generate oligonucleotide-conjugated antibodies have subsequently received increasing interest. Common protocols involve bifunctional linkers that target exposed residues of amino acids on the protein surface.[18–20] However, conjugation stoichiometry is challenging to control depending on the abundance of the reactive surface residue. Other approaches that allow site-specific conjugation rely on guiding the reaction with a complementary template,[21] the incorporation of unnatural amino acids,[22,23] targeting unique or rare amino acids on native proteins[24] or the use of tag-enzyme pairs.[25–28] We previously established the Tub-tag® conjugation technology for bioorthogonal, chemoenzymatic labelling of proteins[29,30] The Tub-tag® technology makes use of the enzyme tubulin tyrosine ligase (TTL) as a highly flexible tool for protein modification, that accepts a broad range of tyrosine derivatives as substrates enabling various bioorthogonal chemistries. We demonstrated its suitability for functionalization with small molecules[31] as well as protein-protein ligation.[32] In this work, we present the Tub-tag® mediated, efficient and site-specific generation of nanobody-DNA and -PNA conjugates in a 1:1 stoichiometry that can readily be used for reversible staining in confocal fluorescence microscopy.

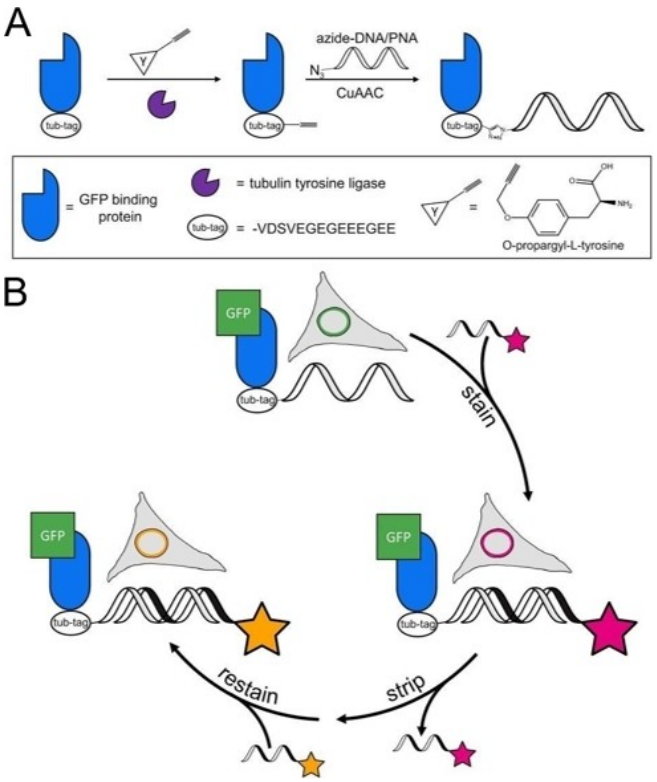

Figure 1. Functionalization strategy for generating nanobody-oligonucleotide conjugates and usage for reversible staining in fluorescence microscopy. A) Schematic representation of the site-specific ligation of single-stranded oligonucleotides to the C terminus of Tub-tagged nanobodies in a two-step process. First, an alkyne handle is introduced by the tubulin-tyrosine ligase (TTL)-catalyzed ligation of *O*-propargyl-L-tyrosine to the Tub-tag. Second, azide-DNA or azide-PNA is conjugated to the alkyne handle by CuAAC. B) Reversible immunofluorescence staining by hybridization of a fluorescent imager strand with the nanobody-oligonucleotide conjugate. Stripping of the imager strand allows for restaining of the sample.

Results and Discussion

Our approach combines enzyme-catalyzed ligation of a reactive chemical handle to an eGFP-binding nanobody (GBP) with Cu^{I}-catalyzed alkyne-azide cycloaddition (CuAAC) to conjugate the oligonucleotide (Figure 1A). As proof-of-principle, we employed these conjugates for reversible staining of eGFP-fusion protein expressing cells in confocal fluorescence microscopy (Figure 1B). In a first step, TTL recognizes the C-terminal Tub-tag® on the protein and site-specifically ligates O-propargyl-L-tyrosine to the C terminus of the antibody. This introduces an alkyne group to the protein that can be used as a chemical handle for following reactions. Second, we used CuAAC for conjugation of an azide-containing DNA or PNA to form a stable bond between antibody and oligonucleotide at a 1:1 stoichiometry. We envisioned that the unique characteristics of PNAs such as higher melting temperature and uncharged backbone would additionally broaden the general applicability of this strategy alternative to DNA conjugation.

We first set out to generate antibody-DNA/-PNA conjugates by using Tub-tag® technology and CuAAC based on previously published optimizations[32] and used eGFP-binding protein as a model antibody fragment. SDS-PAGE and Coomassie staining confirmed efficient conjugation of both azide-DNA (yield: 55.9%) and azide-PNA (yield: 66.1%) to alkyne-modified GBP at 4x molar excess of azide-oligo over nanobody (Figure 2A).

We hypothesized that especially the DNA oligonucleotide would strongly influence the total charge of the conjugated molecule so that unfunctionalized alkynyl GBP can be separated from the conjugate. Therefore, we performed mass spectrometry (Figure S1) and anion-exchange chromatography (AEX) to further validate our observation from the gel electrophoresis. Notably, we observed a strong shift towards higher ionic strength for GBP-DNA conjugate compared to unfunctionalized alkynyl GBP indicating stronger interaction with the stationary phase (Figure 2B). In addition, the GBP-DNA conjugate and free azide-DNA were not separable to baseline, thus suggesting that binding to the stationary phase is mediated by the DNA oligonucleotide to a major degree. Nevertheless, AEX allows for removal of unconjugated alkynyl antibody as demonstrated by SDS-PAGE (Figure 2A) and partial depletion of free DNA in the final product. In contrast, the antibody-PNA conjugates shifted towards lower ionic strengths. In accordance with this observation, free azide-PNA molecules eluted during the column wash because PNA does not have a strong negative charge (Figure 2B).

Taken together, these findings not only confirm that our chemoenzymatic functionalization approach is capable of generating protein-oligonucleotide conjugates with high efficiency, but also that unfunctionalized alkynyl protein is separable from the conjugate product by AEX and free azide-oligonucleotides can be at least partially depleted.

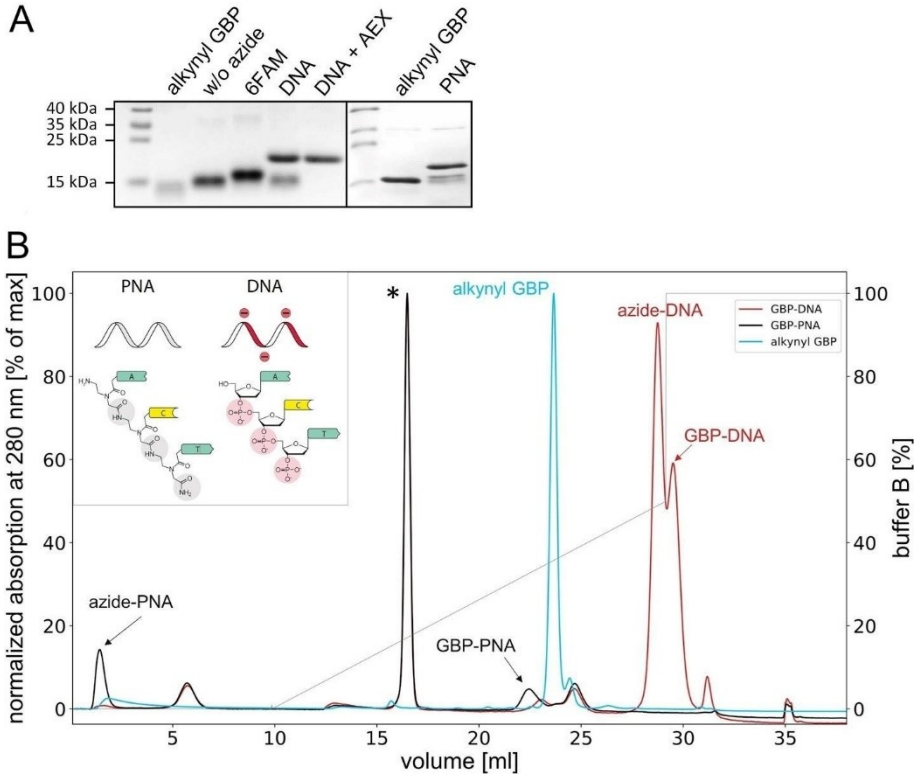

Figure 2. TTL-catalyzed enzymatic incorporation of *O*-propargyl-L-tyrosine and subsequent conjugation of azide-modified 15 bp DNA and PNA strands by CuAAC. A) Coomassie staining of SDS gels of functionalized alkynyl GBP (cropped sections, contrast adjusted, full images can be found in Figure S2). Alkynyl GBP was generated by TTL-catalyzed ligation of *O*-propargyl-L-tyrosine (298 μM GBP-TT, 29.8 μM TTL and 10 mM *O*-propargyl-L-tyrosine for 3 h at 30 °C). Conjugation with azide-DNA was performed by using 40 μM akynyl GBP and 160 μM azide-DNA; conjugation with azide-PNA was performed by using 60 μM alkynyl GBP and 120 μM azide-PNA (0.25 mM $CuSO_4$, 1.25 mM THPTA, 5 mM aminoguanidine and 5 mM sodium ascorbate). B) Analytical anion-exchange chromatography of the raw conjugation products of (A). Absorption (280 nm) is normalized to the strongest signal. The peak marked with an asterisk represents EDTA (Figure S3).

To determine whether the antibody-oligonucleotide can bind both target and the complementary imager strand, we performed an *in vitro* binding assay on immobilized purified protein using either eGFP (target) or BSA (negative control). We detected strong signals for both DNA and PNA conjugate when the sample was hybridized with the complementary imager DNA-strand. Using either BSA as target protein or a non-complementary imager strand lead only to a minor increase of fluorescence (Figure 3 top). This result confirmed that the functionality of both the antibody and the DNA docking strand was preserved by our conjugation strategy, as our conjugate was able to bind both eGFP and the complementary imager strand. Based on these findings, we were prompted to test our conjugate on fixed cells, which provide a much more complex environment that could potentially lead to a higher degree of unspecific staining. Therefore, we used transiently transfected HEK293F cells expressing eGFP-actin fusion protein, and repeated the staining similar to the previous experiment (Figure 3, bottom). We observed the strongest signal in eGFP-actin-transfected cells when staining with the complementary imager strand. Untransfected cells that do not express eGFP did not show elevated levels of fluorescence in the imager strand channel. Staining with noncomplementary imager strand resulted in a minor increase of background fluorescence in both transfected and untransfected cells, suggesting that this effect is inherent to unspecific binding of the DNA or fluorophore itself to cellular components but not due to interaction with the docking strand. Antibody-PNA conjugate yielded higher fluorescence intensity, potentially indicating stronger binding of the DNA imager strand to PNA than to DNA as reported previously.[33]

These promising results encouraged us to test whether the conjugate can be used for reversible immunostaining in confocal fluorescence microscopy. To this end, we stained fixed HEK293F and HeLa cells expressing either eGFP-LaminB1 or eGFP-PCNA fusion proteins, respectively, with DNA-conjugated nanobody. To verify that the imager strand can be detached from the docking strand, we stripped the samples with formamide containing buffer and performed restaining using an imager strand with the same sequence but different fluorophore as visualized in Figure 1B. For both target proteins, we observed distinct nuclear staining with strong colocalization of imager strand and eGFP-LaminB1 or eGFP-PCNA, respectively (Figure 4). After stripping off the first imager strand, we detected practically no remaining fluorescence although we used a highly sensitive detector, thus suggesting that the imager strand was efficiently detached from the DNA-docking strand. Restaining with a second imager strand led again to

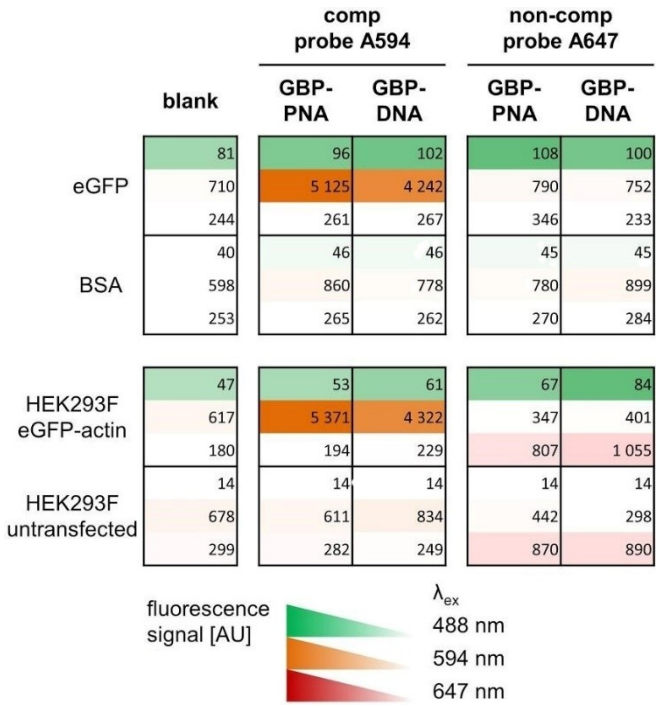

Figure 3. Nanobody-oligonucleotide conjugates exhibit bind to their target protein and allow sequence-specific annealing of fluorescently labelled imager strands. Top: Binding of nanobody-oligonucleotide conjugates to purified eGFP and annealing of a either complementary fluorescent imager strand (comp probe A594) or noncomplementary fluorescent imager strand (non-comp probe A647). Bottom: Binding of nanobody-oligonucleotide conjugates to eGFP-actin expressing cells. Imager strands were used as in the top panels. Fluorescence signal intensity per well is represented by the respective color coding.

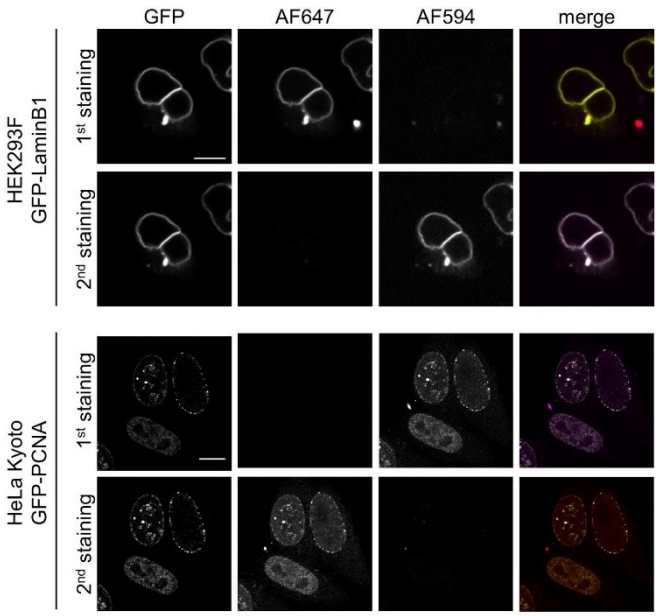

Figure 4. Nanobody-oligonucleotide conjugates are suitable for reversible staining of cells in fluorescence microscopy. Top: Staining of HEK293F cells expressing eGFP-LaminB1. eGFP-LaminB1 is stained by binding of the nanobody-DNA conjugate and subsequent annealing of a complementary imager strand leading to colocalized signal of imager strand and eGFP. Disruption of the interaction of imager and docking strand leads to almost complete removal of fluorescence, allowing for restaining with a complementary imager strand in a different channel. Bottom: Staining of HeLa Kyoto cells expressing eGFP-PCNA. Staining was performed identically to the top panel. Scale bars: 10 μm.

colocalization of eGFP and imager strand fluorescence (Figure 4). Thus, this result demonstrates that the nanobody-DNA conjugate remains intact during the washing and that the staining is reversible. In contrast, nanobody-PNA conjugates showed residual fluorescence after washing in cell staining (Figure S4) as well as *in vitro* binding assays (Figure S5). This observation is potentially due to stronger hybridization of PNA/DNA duplexes and might be resolved by optimization of washing conditions or altering the sequence to lower hybridization temperatures. For nanobody-DNA and -PNA conjugates, we observed minor background staining of the nucleus in all cells even without expression of eGFP (Figure S6); this supports the assumption that the background is likely caused by nonspecific interaction of the DNA-imager strand with genomic DNA.

In summary, we have shown herein a novel conjugation technique for generation of nanobody-DNA and -PNA conjugates. Our approach allows the site-specific conjugation in 1:1 stoichiometry with high efficiency as shown by SDS-PAGE and anion-exchange chromatography. In addition, binding assays on immobilized protein show a strong and specific staining towards the epitope of the antibody. Moreover, we demonstrate quick and efficient reversibility of the staining by using confocal fluorescence microscopy, which is a key requirement for multiplexing via fluorophore exchange. Thus, our technology provides a new tool for chemo-enzymatic generation of protein-oligonucleotide conjugates. The defined 1:1 stoichiometry of our conjugation strategy provides a valuable advantage over currently state-of-the-art functionalization of surface exposed amino acids, where neither the stoichiometry nor the functionalization site is defined.

Acknowledgements

We thank Hans C. Mescheder for countless scientific conversations and critical suggestions contributing to the advancement of this project. Furthermore, we thank Dominik Schumacher for scientific input regarding the Tub-tag® technology. This work was supported by grants from the Deutsche Forschungsgemeinschaft (DFG, German Research Foundation) within the SPP1623 to C.P.R.H. (HA 4468/9-1, 9-2 and 10-2), H.L. (LE 721/13-1, 13-2) and M.C.C. (CA 198/8-1, 8-2), GRK1657/TP1B to M.C.C., GRK1721 to H.L. and the Leibniz Association with the Leibniz Wettbewerb (T18/2017) to C.P.R.H and H.L.. Open access funding enabled and organized by Projekt DEAL.

Keywords: antibody conjugates · immunofluorescence staining · nanobodies · peptide nucleic acids · super-resolution microscopy · Tub-tag labelling

[1] D. Schumacher, C. P. Hackenberger, *Curr. Opin. Chem. Biol.* **2014**, *22*, 62–69.
[2] J. Helma, M. C. Cardoso, S. Muyldermans, H. Leonhardt, *J. Cell Biol.* **2015**, *209*, 633–644.
[3] K. Lang, J. W. Chin, *ACS Chem. Biol.* **2014**, *9*, 16–20.
[4] Z. Zhao, J. Fu, S. Dhakal, A. Johnson-Buck, M. Liu, T. Zhang, N. W. Woodbury, Y. Liu, N. G. Walter, H. Yan, *Nat. Commun.* **2016**, *7*, 10619.
[5] Y. Xiang, Y. Lu, *Nat. Chem.* **2011**, *3*, 697–703.
[6] J. A. G. L. van Buggenum, J. P. Gerlach, S. Eising, L. Schoonen, R. A. P. M. van Eijl, S. E. J. Tanis, M. Hogeweg, N. C. Hubner, J. C. van Hest, K. M. Bonger, K. W. Mulder, *Sci. Rep.* **2016**, *6*, 22675.
[7] J. Wiener, D. Kokotek, S. Rosowski, H. Lickert, M. Meier, *Sci. Rep.* **2020**, *10*, 1457–1457.
[8] C. Hou, S. Guan, R. Wang, W. Zhang, F. Meng, L. Zhao, J. Xu, J. Liu, *J. Phys. Chem. Lett.* **2017**, *8*, 3970–3979.
[9] J. R. McMillan, C. A. Mirkin, *J. Am. Chem. Soc.* **2018**, *140*, 6776–6779.
[10] L. Gogolin, H. Schroeder, A. Itzen, R. S. Goody, C. M. Niemeyer, C. F. W. Becker, *ChemBioChem* **2013**, *14*, 92–99.
[11] S. S. Agasti, Y. Wang, F. Schueder, A. Sukumar, R. Jungmann, P. Yin, *Chem. Sci.* **2017**, *8*, 3080–3091.
[12] F. Schueder, M. T. Strauss, D. Hoerl, J. Schnitzbauer, T. Schlichthaerle, S. Strauss, P. Yin, H. Harz, H. Leonhardt, R. Jungmann, *Angew. Chem. Int. Ed.* **2017**, *56*, 4052–4055; *Angew. Chem.* **2017**, *129*, 4111–4114.
[13] C. Wählby, F. Erlandsson, E. Bengtsson, A. Zetterberg, *Cytometry* **2002**, *47*, 32–41.
[14] K. D. Micheva, S. J. Smith, *Neuron* **2007**, *55*, 25–36.
[15] R. Jungmann, C. Steinhauer, M. Scheible, A. Kuzyk, P. Tinnefeld, F. C. Simmel, *Nano Lett.* **2010**, *10*, 4756–4761.
[16] R. Jungmann, M. S. Avendaño, J. B. Woehrstein, M. Dai, W. M. Shih, P. Yin, *Nat. Methods* **2014**, *11*, 313.
[17] Y. Wang, J. B. Woehrstein, N. Donoghue, M. Dai, M. S. Avendaño, R. C. J. Schackmann, J. J. Zoeller, S. S. H. Wang, P. W. Tillberg, D. Park, S. W. Lapan, E. S. Boyden, J. S. Brugge, P. S. Kaeser, G. M. Church, S. S. Agasti, R. Jungmann, P. Yin, *Nano Lett.* **2017**, *17*, 6131–6139.
[18] C. M. Niemeyer, T. Sano, C. L. Smith, C. R. Cantor, *Nucleic Acids Res.* **1994**, *22*, 5530–5539.
[19] H. Gong, I. Holcomb, A. Ooi, X. Wang, D. Majonis, M. A. Unger, R. Ramakrishnan, *Bioconjugate Chem.* **2016**, *27*, 217–225.
[20] A. V. Maerle, M. A. Simonova, V. D. Pivovarov, D. V. Voronina, P. E. Drobyazina, D. Y. Trofimov, L. P. Alekseev, S. K. Zavriev, D. Y. Ryazantsev, *PLoS One* **2019**, *14*, e0209860.
[21] C. B. Rosen, A. L. B. Kodal, J. S. Nielsen, D. H. Schaffert, C. Scavenius, A. H. Okholm, N. V. Voigt, J. J. Enghild, J. Kjems, T. Tørring, K. V. Gothelf, *Nat. Chem.* **2014**, *6*, 804–809.
[22] K. Lang, J. W. Chin, *Chem. Rev.* **2014**, *114*, 4764–4806.
[23] D. Katrekar, A. M. Moreno, G. Chen, A. Worlikar, P. Mali, *Sci. Rep.* **2018**, *8*, 3589.
[24] M.-A. Kasper, M. Glanz, A. Stengl, M. Penkert, S. Klenk, T. Sauer, D. Schumacher, J. Helma, E. Krause, M. C. Cardoso, H. Leonhardt, C. Hackenberger, *Angew. Chem. Int. Ed.* **2019**, *54*, 11625–11630.
[25] M. W.-L. Popp, J. M. Antos, H. L. Ploegh, *Curr. Protocols Protein Sci.* **2009**, *56*, 15.13.11-15.13.19.
[26] D. Rabuka, J. S. Rush, G. W. deHart, P. Wu, C. R. Bertozzi, *Nat. Protoc.* **2012**, *7*, 1052–1067.
[27] V. Siegmund, S. Schmelz, S. Dickgiesser, J. Beck, A. Ebenig, H. Fittler, H. Frauendorf, B. Piater, U. A. K. Betz, O. Avrutina, A. Scrima, H.-L. Fuchsbauer, H. Kolmar, *Angew. Chem. Int. Ed.* **2015**, *54*, 13420–13424; *Angew. Chem.* **2015**, *127*, 13618–13623.
[28] M. Rashidian, J. K. Dozier, M. D. Distefano, *Bioconjugate Chem.* **2013**, *24*, 1277–1294.
[29] D. Schumacher, J. Helma, F. A. Mann, G. Pichler, F. Natale, E. Krause, M. C. Cardoso, C. P. Hackenberger, H. Leonhardt, *Angew. Chem. Int. Ed.* **2015**, *54*, 13787–13791; *Angew. Chem.* **2015**, *127*, 13992–13996.
[30] D. Schumacher, O. Lemke, J. Helma, L. Gerszonowicz, V. Waller, T. Stoschek, P. M. Durkin, N. Budisa, H. Leonhardt, B. G. Keller, C. P. R. Hackenberger, *Chem. Sci.* **2017**, *8*, 3471–3478.
[31] M. Effenberger, A. Stengl, K. Schober, M. Gerget, M. Kampick, T. R. Müller, D. Schumacher, J. Helma, H. Leonhardt, D. H. Busch, *J. Immunol.* **2019**, ji1801435.
[32] A. Stengl, M. Gerlach, M.-A. Kasper, C. P. R. Hackenberger, H. Leonhardt, D. Schumacher, J. Helma, *Org. Biomol. Chem.* **2019**, *17*, 4964–4969.
[33] M. C. Chakrabarti, F. P. Schwarz, *Nucleic Acids Res.* **1999**, *27*, 4801–4806.

Manuscript received: October 21, 2020
Revised manuscript received: November 17, 2020
Accepted manuscript online: November 18, 2020
Version of record online: December 17, 2020

ChemBioChem

Supporting Information

Site-Specific Antibody Fragment Conjugates for Reversible Staining in Fluorescence Microscopy

Jonathan Schwach, Ksenia Kolobynina, Katharina Brandstetter, Marcus Gerlach, Philipp Ochtrop, Jonas Helma, Christian P. R. Hackenberger, Hartmann Harz, M. Cristina Cardoso, Heinrich Leonhardt, and Andreas Stengl*

Author Contributions

J.S. Data curation:Lead; Methodology:Equal; Visualization:Equal; Writing – original draft:Lead; Writing – review & editing:Equal
K.K. Data curation:Supporting; Methodology:Supporting; Visualization:Equal; Writing – review & editing:Supporting
K.B. Data curation:Equal; Methodology:Equal; Visualization:Equal; Writing – review & editing:Supporting
M.G. Methodology:Supporting; Writing – review & editing:Supporting
P.O. Methodology:Supporting
J.H. Writing – review & editing:Supporting
C.H. Funding acquisition:Equal; Writing – review & editing:Supporting
H.H. Data curation:Supporting; Writing – review & editing:Supporting
M.C. Funding acquisition:Equal; Supervision:Equal; Writing – review & editing:Equal
H.L. Conceptualization:Equal; Funding acquisition:Lead; Project administration:Equal; Supervision:Equal; Writing – review & editing:Equal
A.S. Conceptualization:Equal; Project administration:Equal; Supervision:Equal; Visualization:Equal; Writing – original draft:Equal; Writing – review & editing:Equal

Experimental Procedures

Oligonucleotide sequences

name	sequence 5’ -> 3’ / N -> C	functionalization
DNA docking strand	TAACTGGACTTCATC	5' azide
PNA docking strand	TAACTGGACTTCATC	N-term N3-acetic acid
DNA probe.A594	GATGAAGTCCAGTTA	3' AF594
DNA probe A647	GATGAAGTCCAGTTA	3' AF647
DNA non-complementary	GTTCATGTGCTGATT	3' AF647

5’ azide-DNA docking strand was purchased from metabion. N terminally modified N3-acetic acid PNA docking strand was purchased from Eurogentech. Fluorophore conjugated DNA imager strands were purchased from Eurofins.

TTL expression and purification

Tubulin tyrosine ligase (TTL) was expressed and purified as previously published. [1]

In short, TTL was expressed as a N-terminally His-tagged SUMO-TTL fusion protein in pET28 backbone in *E. coli* BL21(DE3) cells. Expression was induced with 0.5 mM IPTG for 18 h at 18 °C. Cells were lysed for 2 h at 4 °C in TTL binding buffer (20 mM Tris, 250 mM NaCl, 20 mM Imidazole, 3 mM ß-mercaptoethanol, pH 8.2) in the presence of 100 µg/ml lysozyme and 25 µg/ml DNase followed by sonification (7x8 s, 40 % amplitude, Branson Sonifier) and centrifugation at 20.000 g for 30 min, 4 °C for debris removal. Purification was done on an Äkta pure system (GE Healthcare Life Sciences) using a 5 ml HisTrap HP column (GE Healthcare Life Sciences) according to the manufacturer’s instructions. Peak fractions were pooled, desalted on a PD10 column (GE Healthcare Life Sciences) and the buffer exchanged to TTL storage buffer (20 mM MES, 100 mM KCl, 10 mM $MgCl_2$, 50 mM *L*-glutamate, 50 mM *L*-arginine, 3 mM ß-mercaptoethanol, pH 7.0).

Expression of N-terminally His-tagged GBP-TT and eGFP

Green fluorescent protein binding nanobody (GBP) was expressed and purified as previously published. [1]

In short, nanobody was expressed with N-terminal His-tag and C-terminal tub-tag in *E. coli* JM109 cells. Expression was induced with 1 mM IPTG and bacteria incubated at 18 °C, 180 rpm over night. Cells were lysed for 2 h in NiNTA binding buffer (20 mM Tris-HCl, 250 mM NaCl, 20 mM imidazole, pH 8.2) in the presence of 100 µg/ml lysozyme and 25 µg/ml DNase

followed by sonification (7x8 s, 40 % amplitude, Branson Sonifier) and centrifugation at 20.000 g for 30 min, 4 °C for debris removal. Purification was done on an Äkta pure system (GE Healthcare Life Sciences) using a 5 ml HisTrap HP column (GE Healthcare Life Sciences) according to the manufacturer's instructions. Peak fractions were pooled, concentrated in Amicon Ultra Centrifugal Filters (4 ml, 3 NMWL, Merck Millipore) and buffer exchanged to 1x PBS using Zeba Spin desalting columns (7 MWCO). The eluate was injected onto a Superdex 200 Increase 300/10 column (GE Healthcare Life Sciences) at a flow rate of 1 ml/min in PBS. Peak fractions were pooled and concentrated in Amicon Ultra Centrifugal Filters (4 ml, 3 NMWL, Merck Millipore).

His-tagged eGFP was thankfully provided by H. Flaswinkel (LMU Munich, Germany) and expressed and purified in the same manner as described above for GBP-TT.

GBP DNA/PNA conjugation

Conjugation of nanobodies via CuAAC was adapted from a previous publication. [2]

The ligation of O-propargyl-*L*-tyrosine to GBP-TT was catalyzed by the TTL enzyme in TTL reaction buffer (20 mM MOPS, 100 mM KCl, 10 mM $MgCl_2$, 2.5 mM ATP and 5 mM reduced glutathione, pH 7.0) using 298 µM GBP-TT, 29.8 µM TTL and 10 mM O-propargyl-*L*-tyrosine in minimal volume. The reaction was incubated for 3 h at 30 °C and desalted via Zeba Spin desalting columns (7 MWCO, Thermo Fisher Scientific) for removal of excess O-propargyl-*L*-tyrosine.

For conjugation of O-propargyl-*L*-tyrosine-GBP with 3-azido-DNA binding strands (metabion), CuAAC reactions were performed in volumes of up to 115 µl with either 40 µM alkynyl-GBP and 4x excess of azide-DNA for SDS-PAGE and analytical AEX or 70 µM concentration of propargyl-GBP and 2x excess of azide-DNA for preparative AEX in CuAAC reaction buffer (final concentrations in the reaction: 0.25 mM $CuSO_4$, 1.25 mM THPTA, 5 mM aminoguanidine, 5 mM sodium ascorbate, 20 mM MOPS, pH 7.0) for 1 h at 25 °C.The reaction was immediately quenched by the addition of 50 mM EDTA and samples were desalted via Zeba Spin desalting columns (7 MWCO) to 1x PBS. Conjugation with N-terminally modified azido-PNA (Eurogentech) was performed as described above using 60 µM propargyl-GBP with 2x excess of azido-PNA. For control reactions, 10 mM 6-Fluorescein azide (baseclick) were used. Reaction products were analyzed by Coomassie staining and anion exchange chromatography. Reaction efficiency was calculated by densitometric analysis using GelAnalyzer (GelAnalyzer 19.1, www.gelanalyzer.com, by Istvan Lazar Jr., PhD and Istvan Lazar Sr., PhD, CSc)

Purification of nanobody conjugates by anion exchange chromatography

Preparative anion exchange chromatography was performed on an Äkta pure system (GE Healthcare Life Sciences) using a ResourceQ column (Amersham Pharmacia Biotech) equilibrated in buffer A (20 mM MOPS, pH 7.0). Separation was performed by linear increase to 50% buffer B (20 mM MOPS, 1 M NaCl, pH 7.0) over 20 CV followed by 100% buffer B for 5 CV

and protein absorption measured at 280 nm. Peak fractions were collected, concentrated using Amicon Ultra Centrifugal Filters (0.5 ml, 3 NMWL, Merck Millipore) and buffer exchanged to 1x PBS using Zeba Spin desalting columns (7 MWCO).

Quadrupol time-of-flight mass spectrometry of intact proteins

Intact proteins were analyzed using a Waters H-class instrument equipped with a quaternary solvent manager, a Waters sample manager-FTN, a Waters PDA detector and a Waters column manager with an Acquity UPLC protein BEH C4 column (300 Å, 1.7 µm, 2.1 mm x 50 mm). 3 µl of buffered Protein solution were injected and eluted with a flow rate of 0.3 ml/min. The following gradient was used: A: 0.01% FA in H_2O; B: 0.01% FA in MeCN. 5-95% B 0-6 min. Mass analysis was conducted with a Waters XEVO G2-XS QTof analyzer. Proteins were ionized in positive ion mode applying a cone voltage of 40 kV. Raw data was analyzed with MaxEnt 1 and the recorded ion series was deconvoluted for a mass range from 3000 to 25000 Da.

Antigen binding and imager strand annealing/dissociation assay

Purified eGFP (the antigen) was immobilized on 96-well µClear plates multiwell plates (Greiner) at a concentration of 5 µM for 1 h at room temperature. Antigen coated wells and uncoated control wells were blocked with 1% BSA solution for 1 h at room temperature followed by two washing steps with PBST (PBS/0.05 % Tween20). 7.5 µM GBP-PNA and GBP-DNA conjugate were added to for 1 h at room temperature followed by three PBST wash steps. Fluorophore labelled DNA strands (imager strands) with DNA sequences complementary or non-complementary to the GBP-conjugated oligonucleotide were added at 10 µM for 30 min and washed three times with PBST. Fluorescence signal was recorded on a Tecan Infinite 1000 multiwell plate reader system with excitation wavelengths set to 488 nm (eGFP), 603 nm (Atto594) and 646 nm (Atto647) and emission wavelength to 509 nm, 626 nm and 664 nm, respectively. Mean fluorescence intensity of duplicate wells was calculated and depicted as colour intensities.

For *in vitro* cell binding assays, eGFP-actin transfected or untransfected control cells were seeded on 96-well µClear plates multiwell plates (Greiner), fixed and permeabilized as described in the imaging section below. Wells were blocked with 1% BSA solution for 1 h at room temperature followed by two washing steps with PBST (PBS/0.05 % Tween20). 7.5 µM GBP-PNA conjugate were added to for 1 h at room temperature followed by three PBST wash steps. Fluorophore labelled DNA strands (imager strands) with DNA sequences complementary or non-complementary to the GBP-conjugated oligonucleotide were added at 10 µM for 30 min and washed three times with PBST. The annealed imager strand was dissociated by a 2 h wash in PBS/50% formamide, followed by three PBST wash steps. Imager strand was re-annealed for 1 h at room temperature followed by three PBST wash steps. Fluorescence signal was recorded on a Tecan Infinite 1000 multiwell plate reader system with excitation wavelengths set to 603 nm (Atto594) and emission wavelength to 626 nm. Mean fluorescence intensity of duplicate wells was calculated and depicted as colour intensities.

Cell lines generation and cell culture

HEK293Freestyle (Thermo Fisher Scientific) cells were seeded on poly-*L*-lysine coated µ-Slide 8 Well ibiTreat (cat.no 80826, ibidi) containing DMEM/F12 medium (Thermo Fisher Scientific) supplemented with 10% FBS at 40.000 cells per well and incubated at 37 °C in a humidified atmosphere of 5% CO2 to allow attachment. Cells were transiently transfected with plasmid bearing eGFP gene and laminB1 gene (Daigle *et al*., 2001) at DNA concentration of 2.5 µg/ml using MAXreagent (Thermo Fisher Scientific).

The human cervical carcinoma HeLa Kyoto cells (ATCC No. CCL-2), HeLa Kyoto eGFP-PCNA cells, HeLa Kyoto mCherry-PCNA cells, and HeLa Kyoto eGFP-laminB1 cells were grown in DMEM medium supplemented with 10% FCS, L-glutamine and antibiotics at 37 °C in a humidified atmosphere of 5% CO2. HeLa Kyoto cell lines expressing fluorescent PCNA variants were generated in (Chagin *et al*., 2016) using the Flp-In recombinant system. HeLa Kyoto eGFP-laminB1 cells were obtained by transfection with the plasmid bearing eGFP gene and laminB1 gene (Daigle *et al*., 2001). Positively transfected cells were selected visually. Cells were seeded on the µ-Slide 8 Well ibiTreat (cat.no 80826, ibidi) at a concentration 20.000 cells per well. Cells were incubated for 24 h in a humidified atmosphere as described above.

Cell staining with conjugates, imaging and microscopy

eGFP-laminB1 transfected HEK cells were fixed in PBS/4% PFA solution for 10 min at room temperature, washed twice in PBS/0.05% Tween20 (Carl Roth) and permeabilized with PBS/0,25% TritonX-100 (Sigma Aldrich) for 10 min at room temperature. Cells were washed in PBS, blocked in PBS/5% BSA for 1 h at room temperature and incubated overnight at 4 °C with anion exchange purified DNA/PNA conjugated nanobody (16,6 µM in PBS/5% BSA). Samples were washed twice in PBS and stained with 10 nM imager strand for 5 min at room temperature in imaging buffer (500 mM NaCl in PBS, pH 8.0) followed by two washes with imaging buffer prior to imaging. After imaging, samples were washed twice in 0.01x PBS followed by two washes in stripping buffer (PBS/30% formamide for DNA-GBP and PBS/50% formamide for PNA-GBP samples) with 3 min incubation times at room temperature. Samples were washed twice in PBS prior to restaining. For HeLa Kyoto and HeLa Kyoto with fluorescent variants of PCNA and laminB1 the staining procedure was identical as for HEK cells.

For HEK293F cells, spinning disk confocal imaging was carried out on a Nikon TiE microscope equipped with a Yokogawa CSU-W1 spinning disk confocal unit (50 µm pinhole size), an Andor Borealis illumination unit, Andor ALC600 laser beam combiner (405 nm / 488 nm / 561 nm / 640 nm), and Andor IXON 888 Ultra EMCCD camera. The microscope was controlled by software from Nikon (NIS Elements, ver. 5.02.00). Images were acquired with a pixel size of 217 nm using a Nikon CFI Apochromat TIRF 60x NA 1.49 oil immersion objective (Nikon). eGFP, Alexa594 and Alexa647 were excited for 500 ms using the 488, 561 and 640 nm laser lines, respectively. The emission of eGFP, Alexa594 and Alexa647 was captured by using a 525/50 nm, a 600/50 nm and a 700/75 nm filter, respectively. In addition, differential interference contrast (DIC) images were acquired. Confocal microscopy images of HeLa Kyoto cells were acquired using a Leica TCS

SP5II confocal laser scanning microscope (Leica Microsystems, Wetzlar, Germany) equipped with an oil immersion Plan-Apochromat x100/1.44 NA objective lens (pixel size in XY set to 100 nm, Z-step=290 nm) and laser lines at 488, 561 and 633 nm. For the second round of imaging cells were recorded as z-stacks with a z-spacing of 290 nm to find the exact plane corresponding to the first round of imaging.

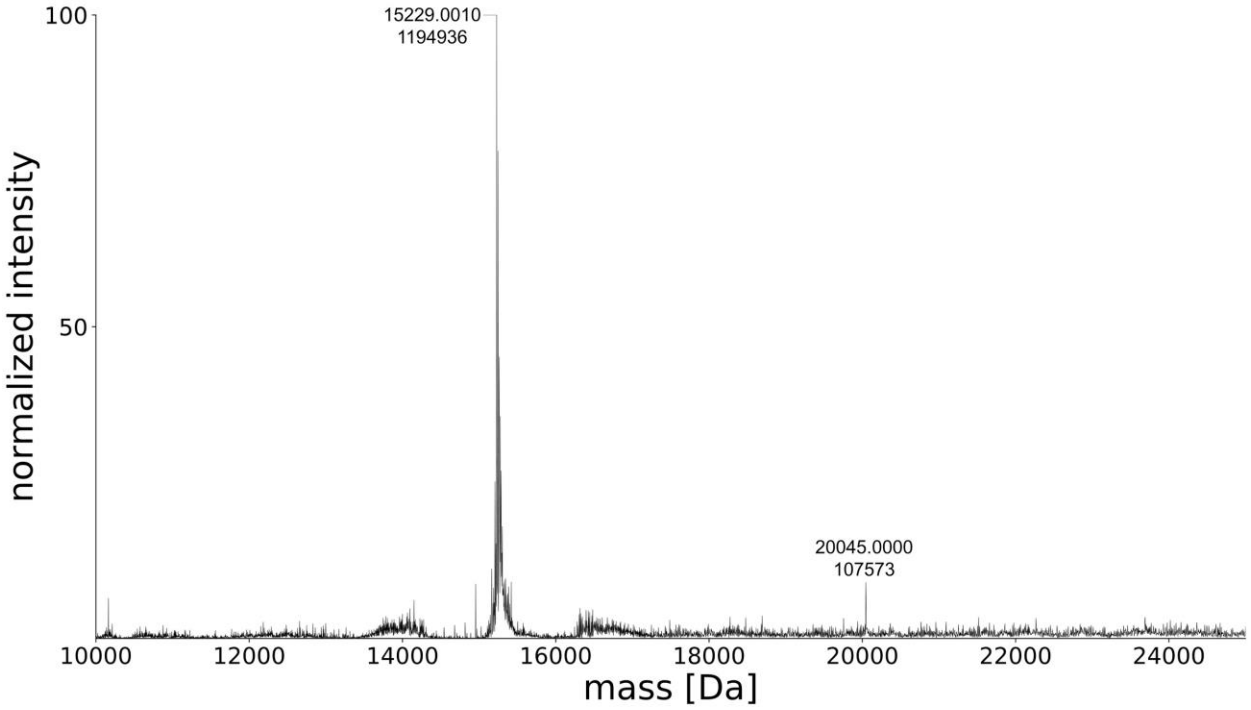

Figure S1: Quadrupol time-of-flight mass spectrometry of alkynyl GBP functionalized with azide-DNA. Calculated mass of alkynyl-GBP: 15229 Da. Calculated mass of GBP-DNA conjugate: 20045 Da (15229 Da alkynyl GBP + 4816 Da of azide-DNA).

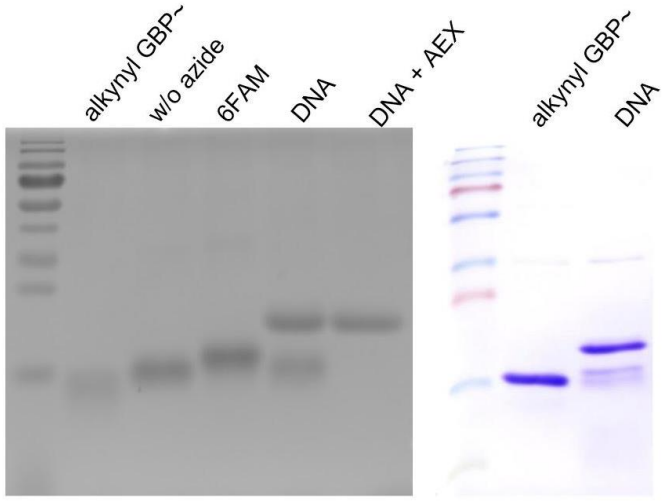

Figure S2: Uncropped and unadjusted images of coomassie stained SDS gels. Left image was recorded in grayscale right image in color mode. SDS-PAGE analysis of functionalized alkynyl GBP as shown in Figure 2A. Alkynyl GBP was generated by TTL catalyzed ligation of O-propargyl-*L*-tyrosine (298 µM GBP-TT, 29.8 µM TTL and 10 mM O-propargyl-*L*-tyrosine for 3 h at 30 °C). Conjugation with azide-DNA was performed using 40 µM akynyl GBP and 160 µM azide-DNA; conjugation with azide-PNA was performed using 60 µM alkynyl GBP and 120 µM azide-PNA (0.25 mM $CuSO_4$, 1.25 mM THPTA, 5 mM aminoguanidine and 5 mM sodium ascorbate).

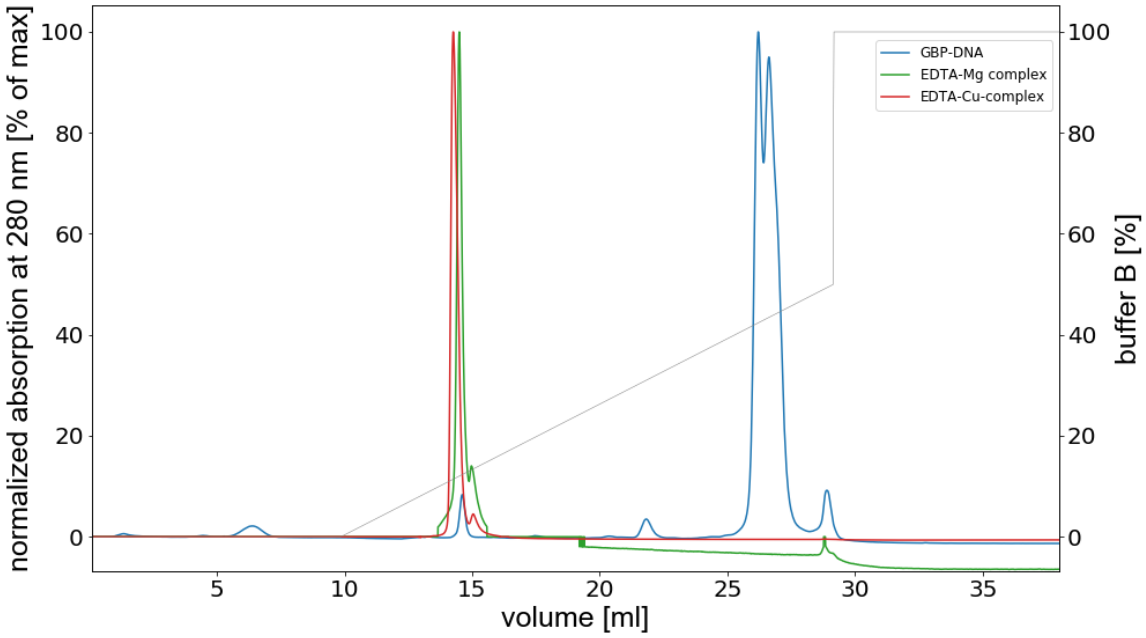

Figure S3: Anion exchange chromatography of EDTA in complex with Cu or Mg ions. Overlay of EDTA chromatograms with GBP-DNA conjugate chromatogram shows elution of residual EDTA that was added for competitive complexation of Cu ions in the buffer exchanged conjugation product

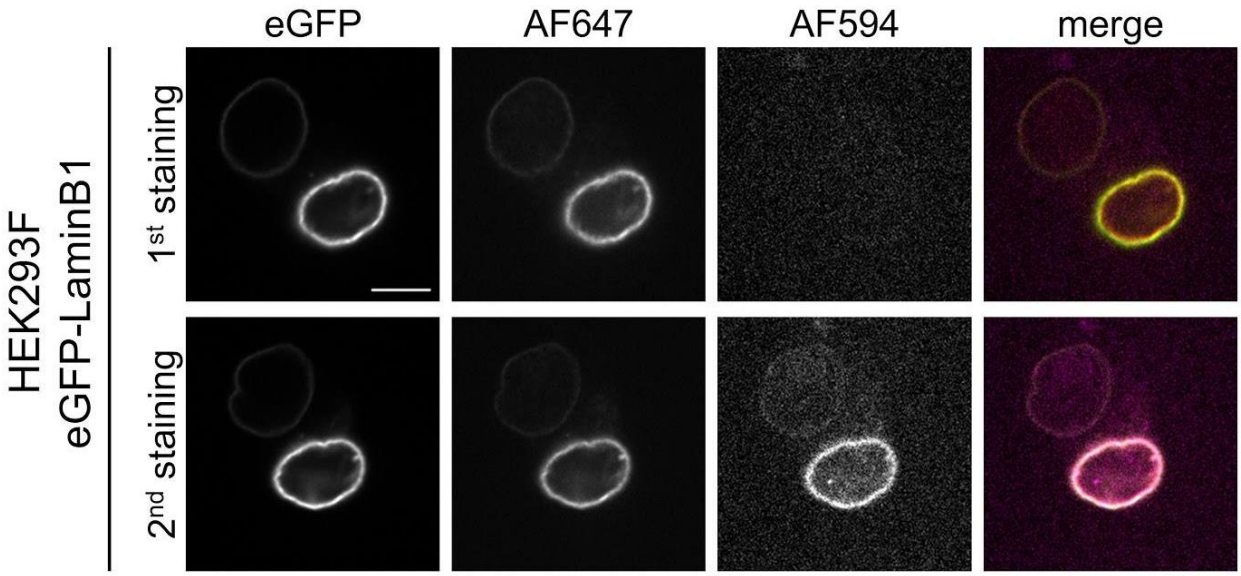

Figure S4. Staining of HEK293F cells expressing eGFP-Lamin. eGFP-LaminB1 is stained by binding of the nanobody-PNA conjugate and subsequent annealing of a complementary imager strand leading to colocalized signals of imager strand and eGFP. Attempted disruption under the same conditions as for nanobody-DNA conjugate does not lead to a major decrease in fluorescence. However, annealing of a second imager strand leads to additional signal in the respective channel. Scale bar represents 10 µm.

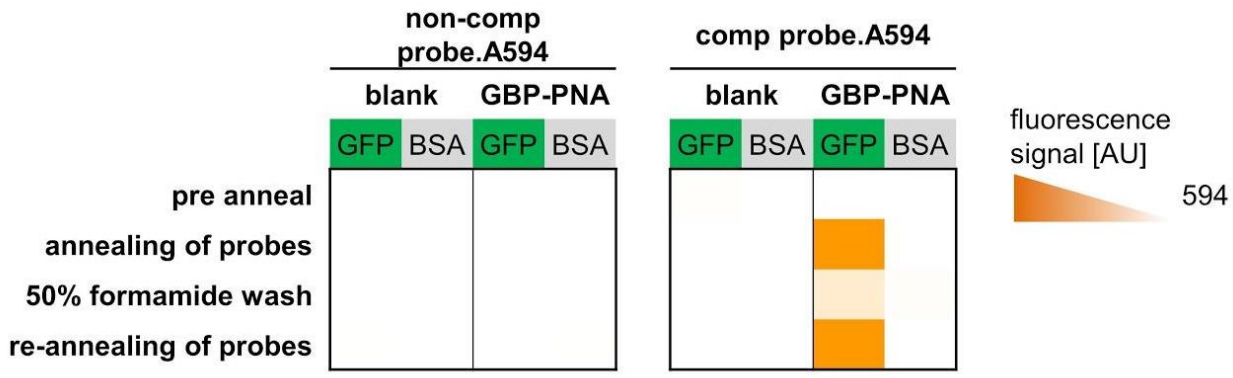

Figure S5. *In vitro* binding assay of GBP-PNA conjugates. Sequence-specific binding of imager strands to GBP-PNA conjugates bound to immobilized eGFP and reversible annealing of fluorescent imager strands. Disruption with formamide leads to an incomplete decrease in fluorescence. Fluorescence signal intensity per well is represented by the respective colour coding.

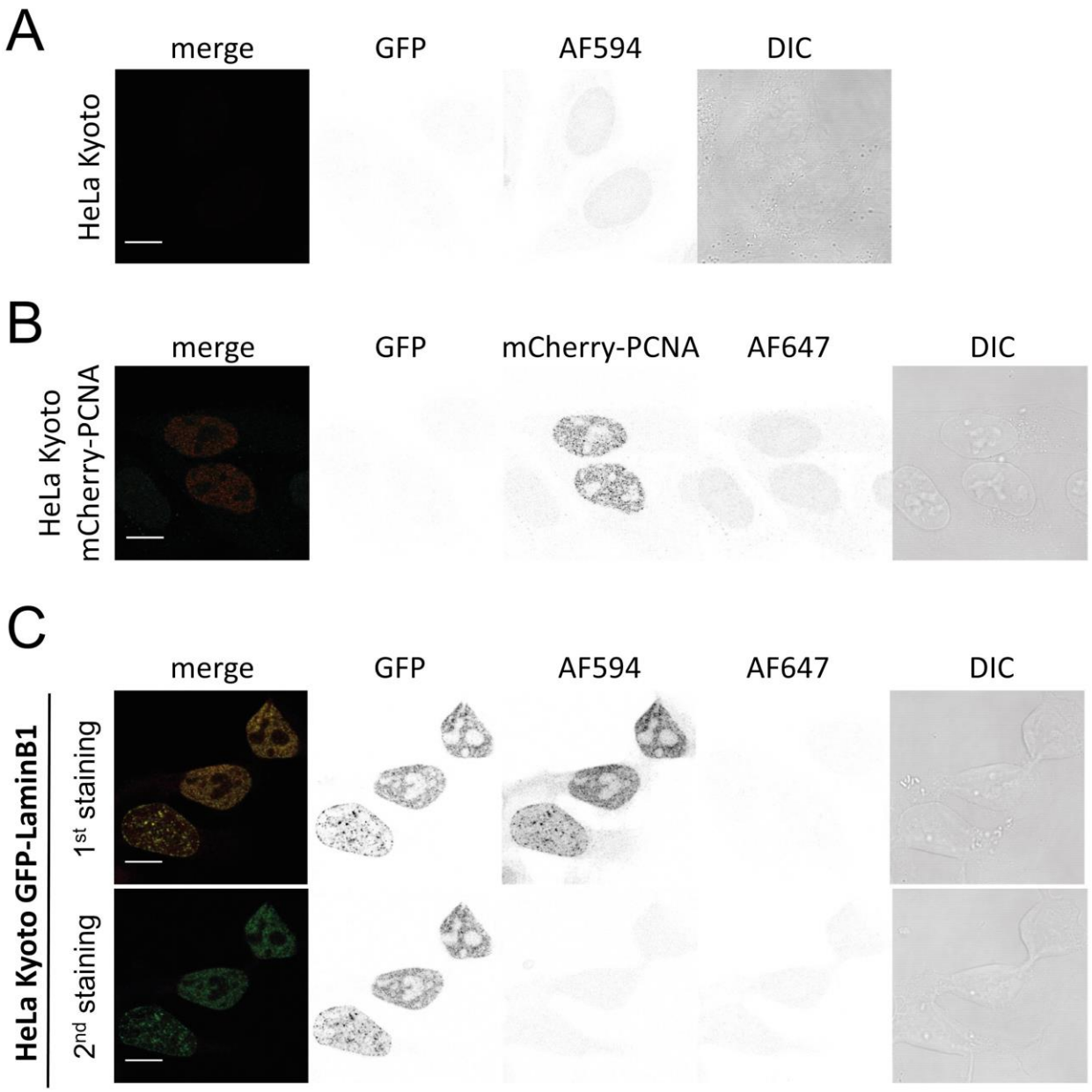

Figure S6. HeLa Kyoto cell lines expressing (A) no fluorescent protein, treated with GBP-DNA conjugate followed by addition of complementary imager strand (AF594), (B) mCherry-PCNA fusion protein, treated with GBP-DNA conjugate followed by addition of complementary imager strand (AF647) or (C) GFP-LaminB1, treated with GBP-DNA conjugate followed by addition of complementary (AF594) and non-complementary (AF647) imager strand (1st and 2nd staining, respectively). Staining with nanobody-DNA conjugate and subsequent annealing of imager strand leads to a minor, non-specific background signal especially within the nucleus. Expression of mCherry-PCNA does not lead to colocalization of mCherry and imager strand. Expression of GFP and binding of GBP-DNA conjugate enables specific binding of complementary imager strand, but not a non-complementary sequence. Scale bars represent 10 µm.

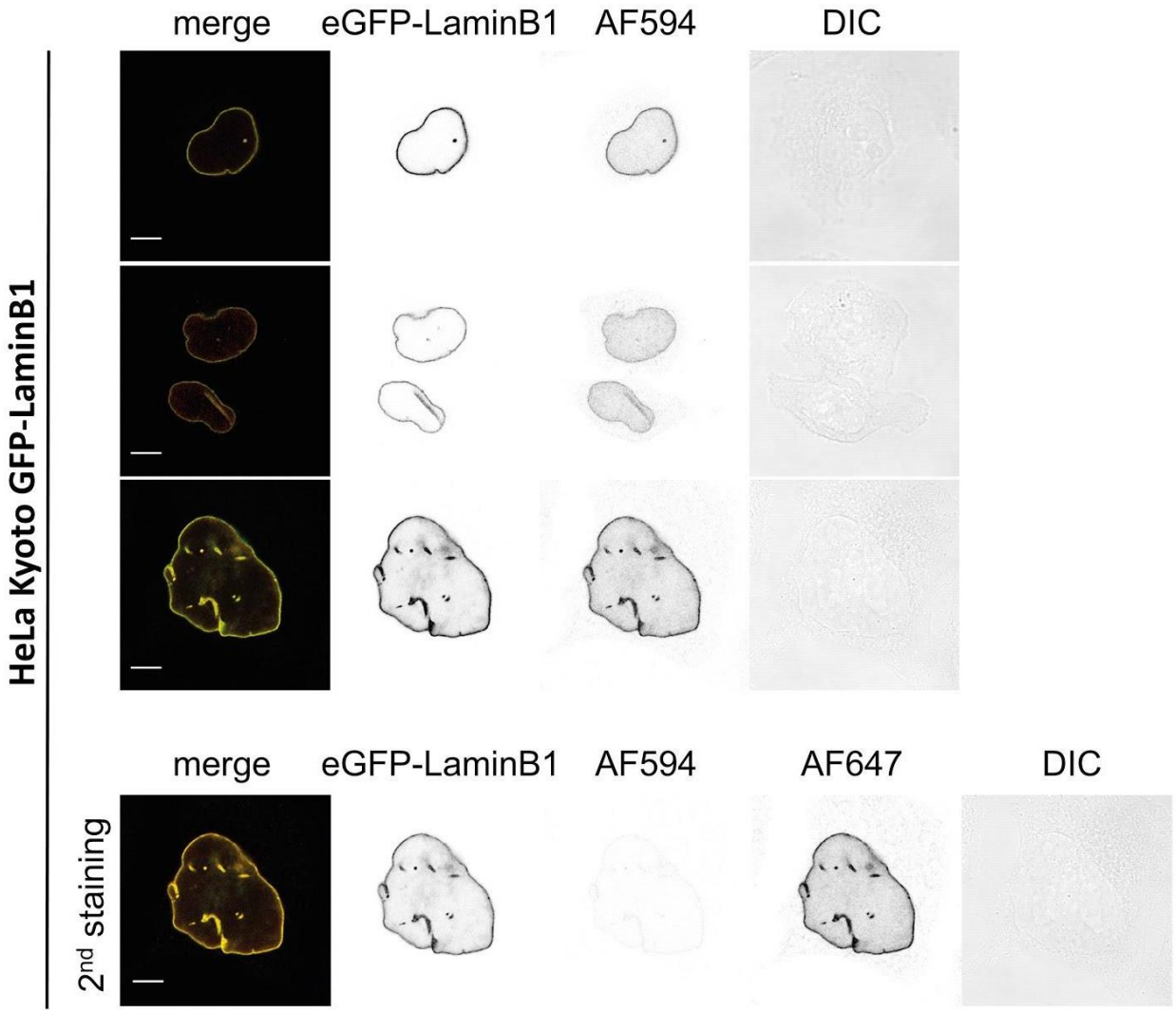

Figure S7. Staining of HeLa Kyoto cells expressing eGFP-LaminB1. eGFP-LaminB1 was stained by binding of the nanobody-DNA conjugate and subsequent annealing of a complementary imager strand leading to colocalized signals of imager strand and eGFP. Disruption of the interaction of imager and docking strand leads to almost complete loss of fluorescence, allowing for restaining with a complementary imager strand detectable in a different channel (bottom panels). Scale bars represent 10 µm.

References

[1] D. Schumacher, J. Helma, F. A. Mann, G. Pichler, F. Natale, E. Krause, M. C. Cardoso, C. P. Hackenberger, H. Leonhardt, *Angewandte Chemie International Edition* **2015**, *54*, 13787-13791.

[2] A. Stengl, M. Gerlach, M.-A. Kasper, C. P. R. Hackenberger, H. Leonhardt, D. Schumacher, J. Helma, *Organic & Biomolecular Chemistry* **2019**, *17*, 4964-4969.